SPE 71700

Temperature effect on NMR surface relaxation

S. Godefroy, M. Fleury, and F. Deflandre, IFP, France, and J.-P. Korb, LPMC, Ecole Polytechnique, France

This paper was prepared for presentation at the 2001 SPE Annual Technical Conference and Exhibition held in New Orleans, Louisiana, 30 September–3 October 2001.

Abstract

We present NMR relaxation experiments of water and oil confined in a series of calibrated porous media and natural rocks of different wettability, at various temperatures and magnetic fields. The longitudinal $1/T_1$ and transverse $1/T_2$ relaxation rates are interpreted with an original theoretical model which shows that the solid-liquid interactions occurring at the grain surface are responsible for the temperature dependence of the relaxation rates. For instance, $1/T_1$ and $1/T_2$ measured on water saturated samples of silica surfaces present an anomalous temperature behavior, contrary to the case of water in porous media with calcium carbonate surfaces. The relaxation rates of oil saturated porous media present always a normal temperature behavior for every surface. The temperature effect is not negligible for high reservoir temperature and should be taken into account or tested when calibrating log data using experiments performed at laboratory temperature.

Introduction

Nuclear Magnetic Resonance (NMR) well logging is now used routinely to determine the fundamental properties of reservoir rocks, such as porosity, saturation, and permeability[1]. From relaxation time distributions, this technique allows in particular the determination of irreducible water saturation[2]. However, a calibration based on laboratory data is often necessary and these data are collected at room temperature. In general, NMR phenomena are sensitive to temperature and the validity of the calibration from laboratory data might be discussed. Published experiments on temperature dependence of the NMR parameters have shown weak and negligible temperature effect for water in natural rocks with a relatively broad pore size distributions[3]. We showed in a previous work, based on experiments performed on calibrated porous media, a particular temperature dependence of these parameters, depending on the nature of the liquid and the pore surface[4]. Here we consider the temperature effect on a large variety of samples, from grain packing to outcrop and reservoir samples of intermediate wettability.

Basically, the principle of NMR relaxation in porous media consists in the measurement (*in-situ* or in the laboratory) of the transverse, $1/T_2$, relaxation rates of the liquid (water and oil) saturating the porous media. In the case of NMR measurements while drilling, the longitudinal, $1/T_1$, relaxation rate is preferred for various technical reasons. These rates are generally related to the surface to volume ratio (S/V) of the pore, and are given by the general expression:

$$\frac{1}{T_{1,2}} = \frac{1}{T_{1,2B}} + r_{1,2}\frac{S}{V} \qquad (1)$$

In this expression, $1/T_{1B}$ and $1/T_{2B}$ are the bulk longitudinal and transverse relaxation rates, respectively. ρ_1 and ρ_2 are the surface longitudinal and transverse relaxivity parameters, respectively. These two times, T_1 and T_2, are measured by NMR radio-frequency pulse sequences very well documented in the literature[5]. The surface relaxivities ρ_1 and ρ_2 depend both on the surface and liquid characteristics and an important literature can be found on water relaxivity on various surfaces[1,6]. For petroleum applications, the relaxivity of oil must also be considered due to the existence of oil-wet surfaces in many reservoir rocks[7]. Therefore, both water and oil relaxation times can be dominated by surface interactions and potentially depend on temperature.

In this paper, we first outline our theoretical frequency and temperature dependence of surface relaxivity $\rho_{1,2}$ in porous media[4]. The temperature dependence of the relaxation rates that we obtain on water or oil (dodecane) saturated calibrated grain packings support our theory. Finally, we present similar experiments perfomed on natural (outcrop and reservoir) rocks, which exhibit similar temperature dependence. We discuss also the potential impact of this study for well logging applications.

Theoretical Background and Experiments on Model Porous Media

Frequency and temperature dependence of surface relaxivity. We consider a large number of protons (I) spin – bearing molecules (water or oil) diffusing in pores with a surface density σ_S of fixed paramagnetic impurities (S) (Fig. 1). The gyromagnetic ratio of the electron, γ_S, being much larger than that of the proton, γ_I, ($\gamma_S = 658.21\ \gamma_I$) the proton relaxation is due to the modulation of the dipole-dipole interactions between I and S spins by translational diffusion[5,8]. The situation has been well documented for the case of bulk liquids[5] and general statements have been proposed for the case of porous media[1,6,9]. However the confinement effect that occurs in porous media as well as the surface diffusion of liquids requires another theoretical approach. This is particularly important at low magnetic field in NMR well logging applications, where the surface molecular dynamics is probed on a much wider time scale. We have recently addressed this problem on the basis of the following considerations[4].

(i) The biphasic fast exchange between the surface and the bulk molecules, even in macroporous media where the surface to volume ratio S/V is very small, enhances drastically the surface contribution in Eq. (1).

(ii) The main contribution of the proton relaxation comes from the two dimensional motion of the molecules at the pore surface near the fixed relaxing sinks S.

(iii) The numerous two-dimensional I-S reencounters are responsible for the net frequency dependence observed for the longitudinal spin-relaxation rates.

(iv) The residence time of the studied liquid at the pore surface depends on the existence of potential chemical bonds with specific surface groups.

(v) We introduce two correlation times in the theory. The translational correlation time, defined as t_m, is associated to individual molecular jumps at the surface. The surface residence time, defined as t_s, is limited by molecular desorption. A schematic description of the molecular surface motion is presented on Fig. 1. All these considerations leads, after some calculations detailed in ref. 4, 10 and 11, to the following logarithmic expression of the longitudinal surface relaxavity at low frequency:

$$r_1(w_I, T) = a\, t_m \ln\left[\frac{1 + w_I^2 t_m^2}{(t_m / t_S)^2 + w_I^2 t_m^2}\right] \qquad (2)$$

Here α, defined in ref. 4, depends on parameters characteristics of the liquid and the pore, such as the surface density of paramagnetic impurities σ_S. Such a logarithmic frequency dependence has been experimentally evidenced in calibrated porous media by using the field cycling NMR method[4]. In the following, we focus on the temperature dependence of the surface relaxivity, which comes directly from the correlation times:

$$t_m(T) = t_{m0} \exp\frac{\Delta E}{RT}, \qquad (3)$$

where $\Delta E = E_m - E_s$ is an effective activation energy describing the surface translational motion, R is the gas constant, and T is the temperature (K). $E_m \approx 4.8$ kcal/mol is the activation energy associated to the individual molecular diffusing jumps. E_s is the activation energy associated to the surface chemical bonding. When the diffusing barrier is larger than the bonding energy, namely when $\Delta E>0$, one expects a normal temperature dependence of the surface relaxivity, i.e. ρ_1 decreases with the temperature T. On the contrary, when the diffusion barrier is smaller than the bonding energy, $\Delta E<0$, one expects an anomalous temperature dependence where ρ_1 increases with temperature. When considering the transverse surface relaxivity ρ_2, the frequency dependence is much weaker but the temperature dependence is similar and proportional to the translational correlation time:

$$r_2(T) \propto a\, t_m(T) \qquad (4)$$

where α is a coefficient defined in ref. 4. In consequence the expected temperature dependence of ρ_2 is the same as the one described above.

Experimental validation on model porous media

Methods. The frequency dependence of the longitudinal relaxation rates, $1/T_1$, measured on different systems gives a strong experimental support of Eq. 2 and is described in detail elsewhere[4]. Here, we focus on the temperature dependence and we present experiments performed on three different instruments. We have used a magnetic field cycling instrument of the Redfield design[12], to measure $1/T_1$ for frequencies varying in the range 0.01–30 MHz, at different temperatures. The experiments were performed on a homemade field cycling instrument at the R. G. Bryant's laboratory, (Charlottesville), and on a fast field cycling, Stelar instrument (Italy) at Ecole Polytechnique (France). We measured the transverse relaxation times, T_2, at 2.2 MHz on a Resonance Instrument (England) Maran-2 spectrometer, using a standard spin-echo CPMG sequence[5], at IFP (France). The magnetization decay curves are analyzed using a multi-exponential decomposition process with an optimum smoothing procedure. When possible, relaxation data were also analyzed by using a simple exponential fit to determine the mean relaxation times, therefore increasing the accuracy of the measurements. The variation of T_2 as a function of the temperature was obtained by using a special cell described in Appendix, allowing temperature measurements from 10 up to 100°C.

The different samples were selected principally for their narrow pore size distribution, allowing a much easier study of the temperature effect than in porous media with broad pore size distribution, where the temperature effect can be dominated by the pore coupling. The samples were saturated

either with water or oil (dodecane) using vacuum line techniques.

Materials. The first kind of samples consists in a series of packing of size-calibrated grains. Nonporous silicon carbide, SiC, grains (from Peter Wolters, Germany) were packed using different grain diameters varying in the range 8-150 μm. The packing procedure provided a series of porous media with pore sizes approximately the same as the grain sizes and with a porosity of about 45%. X-ray photoelectron spectroscopy (XPS)[13] have shown that SiO_2 covers 25% of the grain surface, representing hydrophilic zones. The narrow pore size distribution is evidenced by the observed narrow transverse relaxation times (T_2) distribution, as presented on Fig. 2 for the water saturated 8 μm grain packing. Due to the grain preparation, the surfaces contain paramagnetic impurities that originate either from the grinding process or derived from the silicon carbide synthesis. We removed the grinding impurities by applying a continuous flux of hydrochloric acid into the porous media for a few weeks. Electron Spin resonance (ESR) experiments performed on the dry grains after cleaning showed that ferric ions (Fe^{3+}) remained in the grains.

The second kind of sample is a packing of calcite ($CaCO_3$) grains. These grains (Mikhart SPL, from Provencale, France) have an analytical grade of 99.1%. The largest grain diameter is 50 μm, with a mean diameter of 20 μm. We obtained a porosity of 43% for the granular packing. The presence of Mn^{2+} paramagnetic ions has been evidenced by Electron Spin Resonance (ESR).

Results. We display on Fig. 3 (a) and (b) the temperature dependence of $1/T_1$, at different frequencies, for the 100 % water or 100% oil saturated 8 μm grain packing. The temperature dependence of $1/T_1$ for water, below 10 MHz (Fig. 3 (a)), is opposite to that obtained either for bulk water, or oil in the packing (Fig. 3 (b)). As described in the theoretical section, this unusual situation where $1/T_1$ increases with the temperature is due to the hydrogen bonds of water with the numerous silanol groups at the silica pore surface. In fact the low value of the measured effective activation energy $\Delta E \approx -2$ kcal/mol, obtained from the slopes of the curves in Fig. 3 (a), is representative of the proton exchange occurring at the pore surface between the silanol groups and the first hydration shell of water[4]. For oil (dodecane), the measured mean activation energy on the surface, about +2 kcal/mol, is much closer than that of bulk oil (+2.6 kcal/mol). Here, we observe a normal temperature behavior of the relaxation rate, which indicates a pure translational diffusion.

In complement, we measured the temperature dependence of the proton transverse relaxation rates, $1/T_2$, of the water saturated grain packs for the different pore sizes (ranging from 8 to 150 μm) (Fig. 4). In order to emphasize the anomalous temperature dependence of the surface contribution of $1/T_2$, we have corrected the measured relaxation rates from the bulk contribution according to the equation:

$$\frac{1}{T_{2corr}} = \frac{1}{T_2} - \frac{1}{T_{2B}} \qquad (5)$$

The results obtained confirm the observed anomalous temperature dependence obtained for $1/T_1$. In particular, we find the same activation energy $\Delta E \approx -2$ kcal/mol. More generally, these results prove again the anomalous temperature dependence of ρ_2 for water on silica surfaces, as described in the theoretical section.

Of course the physical chemistry on the liquid-solid interface is of particular importance. For instance, one observes a normal temperature dependence of $1/T_2$ for water saturated grain packing of calcite (Fig. 5), with an effective activation energy of $\Delta E \approx 1.9$ kcal/mol.

Temperature experiments on natural porous rocks

In the following, we apply the method described above on two outcrop and reservoir sandstone samples and two outcrop and reservoir carbonate samples, saturated either with water or oil. The samples were selected such as to avoid a high clay content (sandstone) or a bimodal distribution (carbonate). Therefore, the temperature effect can be associated to surface relaxivity and not to pore coupling. The reservoir samples are of intermediate wettability.

Core samples.

Sandstone rocks. The outcrop sandstone studied is a Clashash sandstone of porosity 17 % and water permeability of about 500 mD. From mercury porosimetry, the pore throat radius distribution is narrow. The clay content is very small, as shown by T_2 relaxation time distribution measurements.

The reservoir sandstone studied has a porosity of 19 % and a water permeability of 840 mD. Electronic microscopy has shown that the rock is composed of quartz grain of diameter varying from 30 to 500 μm, sometimes cemented by carbonate. One notes that some of the pores are filled with clays (principally kaolinite). However, the clay bound water measured by NMR represent at most 2% of the total porosity. From mercury porosimetry, the pore throat radius distribution is very narrow and peak at 14 μm. The sample has been cleaned according to IFP's standard procedure and then aged in reservoir crude oil for 3 weeks at elevated temperature[7]. The USBM wettability test performed after aging indicates a wettability index of -0.19, with no spontaneous drainage or imbibition.

Carbonates. The outcrop carbonate used is a fine grain Lavoux limestone of porosity 23 % and water permeability around 3 mD. This limestone rock is typical of a water-wet $CaCO_3$ surface. The narrow pore size distribution of the rock is evidenced by the narrow T_2 distribution of the water saturated sample measured at 2.2 MHz[4]. Mercury porosimetry experiments indicate a mean pore throat radius of 0.5 μm. ESR measurements performed on this rock have shown the presence of Mn^{2+} paramagnetic impurities.

The reservoir carbonate sample studied has a porosity of 24% and a water permeability of 1.5 mD. Electronic microscopy of this rock exhibits the presence of crystals of $CaCO_3$ varying in size from 1 to 20 µm. From mercury porosimetry, the pore throat radius distribution is narrow and peak at 0.5 µm. Electron Spin Resonance (ESR) experiments have shown the presence of Mn^{2+} paramagnetic ions. The sample has been cleaned according to IFP's standard procedure[7]. The USBM wettability test performed after cleaning indicates a wettability index of +0.50. During the wettability test, a spontaneous imbibition of water was observed but the cleaning procedure was not sufficient to remove some absorbed components from the surface, resulting in a non-strongly water-wet state.

Results. We analyze in this section a series of experimental data that prove that the concepts introduced above for model porous media can be extended to describe the temperature dependence of the relaxation rates of water and oil in natural rocks.

Sandstone rocks. For the Clashash outcrop sandstone 100% saturated with water, the variation of the transverse relaxation time distributions, T_2, measured at 2,2 MHz as a function of the temperature is presented in Fig. 6 (a). The general tendency is an anomalous temperature behavior where the relaxation times decrease with temperature. The Fig. 6 (b) presents the Arrhenius diagram of the variation of $1/T_2$, corresponding to the peak relaxation times T_2 (given in table 1) of the distributions described in Fig. 6 (a). From the Arrhenius diagram of the corrected values (Eq. (5)), we measure an effective activation energy $\Delta E \approx -2$ kcal/mol. This result is confirmed from the variation of $1/T_1$ of water in this rock as a function of the temperature, and for different frequencies, obtained by the field cycling technique and presented in Fig. 7.

For the reservoir sandstone moderately oil wet (Iw=-0.19) 100% saturated with water, the transverse relaxation time distributions are presented in Fig. 8 (a), for different temperatures. The general tendency, is also a anomalous decrease of the water relaxation times with increasing temperature, but weaker than for the outcrop sandstone. The values of the peak relaxation times corresponding to the distributions of Fig. 8 (a) are given in table 2. The Fig. 8 (b) shows the Arrhenius diagram of $1/T_2$ of water in this sandstone. When corrected for the bulk values (Eq. (5)), one measures an effective activation energy of $\Delta E \approx -1.7$ kcal/mol.

For the reservoir sandstone 100% oil saturated, the transverse relaxation time distributions, measured at 2,2 MHz and for different temperatures, are shown in the the Fig. 9 (a). One can see a normal temperature dependence of $1/T_2$, corresponding to the relaxation times of the peaks of the distributions. Note that, on this oil-wet surface, oil relaxation times are smaller than the bulk's one, indicating an efficient surface relaxivity. From the slope of the curve of Fig. 9 (b), one obtains $\Delta E \approx 1.5$ kcal/mol.

Carbonates. For the outcrop limestone, on Fig. 10 (a) and (b) are presented, the normal temperature dependence of the longitudinal relaxation rates of water and oil, respectively, saturating the core. Both water and oil relaxation rates follow the same temperature dependence, that is to say decrease with increasing temperatures. For water, one measures a mean effective activation energy of 2.5 kcal/mol.

For the reservoir carbonate, we plotted in Fig. 11 (a) the variation of the transverse relaxation time distribution (at 2.2 MHz) of water saturating the core at 100%, as a function of the temperature. As for the limestone rocks, relaxation times increase with the temperature. The mean relaxation times, T_2, corresponding to the middle of the distribution peaks, are given in Table 3 for the different temperatures. The Arrhenius diagram of Fig. 11 (b), of $1/T_2$, leads to a measured activation energy of $\Delta E \approx 1.9$ kcal/mol.

For this reservoir carbonate, the variation as a function of the temperature of the longitudinal relaxation rates, $1/T_1$, measured at different Larmor frequencies using the field cycling technique, are presented in the Fig. 12 (a) and Fig. 12 (b), of water and oil, respectively, saturating the core at 100%. One measures about the same activation energy for water than the one given by $1/T_2$, and an activation energy of 2.4 kcal/mol for oil.

Discussion and application to log calibration. From the various experiments described above, we can observe general trends describing the temperature dependence of the surface relaxivity (Table 4). For water- or oil-wet surfaces composed mainly of silica, (SiC grain packing, Clashash and reservoir sandstones), the water surface relaxivity parameters increase with temperature according to Eq. 2 to 4, with an observed effective activation energy in the range [-2; –1.7 kcal/mol], and the oil surface relaxivity parameters decrease with temperature with an observed effective activation energy in the range [1.5; 2 kcal/mol]. For water-wet or weakly water-wet surfaces composed mainly of $CaCO_3$ (calcite grain packing, Lavoux limestone and reservoir carbonate), the water or oil surface relaxivity decreases with temperature with an effective activation energy in the range [1.9; 2.5 kcal/mol]. Note that we used a refined oil (dodecane) as the oil phase to determine the oil surface relaxivity. More complex fluids (mud oil filtrate or native crude oil) might complicate the analysis but the general trends should still be valid.

When laboratory and log data are compared in similar saturation conditions (i.e. at 100% water saturation for a water based drilling mud, or at oil-water irreducible water saturation for an oil based drilling mud), the relaxation times might be shifted by a factor equal to the right exponential term in Eq. 3. For instance, from 25 °C up to 120°C, a shift of a factor of 2.1 is possible (taking ΔE = 2kcal/mol), either in reducing or increasing the relaxation times depending on the type of surface. In practice, the temperature effect might be hindered by pore coupling when considering bimodal pore structures, or by mixed surface composition (quartz and calcite). There are

also further complications related to the existence of static magnetic field gradient present in the logging tools that prevent the measurements of long relaxation times,

This work also predict a strong impact on the T_2 cut-off values determined in the laboratory and applied on the log data in the case of high reservoir temperatures. If the relaxation times are shifted, the T_2 cut-off value should also be modified according to:

$$T_{2cutoff} = T_{2cutofflab} \exp\left(-\frac{\Delta E}{R}\left(\frac{1}{T_r} - \frac{1}{T_l} \right) \right) \qquad (6)$$

Here, $T_{2cutofflab}$ is the relaxation time measured in the laboratory, at the temperature T_l (in K), T_r is the reservoir temperature, and ΔE depends on the nature of the surface of the rock considered. Table 4 might be used to estimate orders of magnitude. Hence, if problems are encountered to calibrate logs from laboratory data, the possible shift due to temperature should be considered. Due to the extreme variety of rock surface, it is however recommended to test the temperature effect for each facies or rock type.

Conclusion

On the basis of temperature dependence measurements of NMR relaxation times and a theoretical description of the solid-liquid interactions occurring at the pore surface, we have evidenced two different kinds of temperature dependence of the relaxation times of liquids in pores. The temperature dependence of the relaxation times of water confined in pores with silica surface is anomalous, that is to say, decrease with increasing temperature. On the other hand, relaxation times of oil in pores with silica surface increase with temperature. Relaxation times of water and oil in pores with calcium carbonate surface both increase with increasing temperature. The consideration of these characteristic temperature behaviors can be used as guidelines to compare NMR well logging data acquired at elevated temperature and laboratory experiments performed at room temperature.

Nomenclature

γ_I = proton gyromagnetic ratio
γ_S = electronic gyromagnetic ratio
ν = Larmor frequency
ρ_1 = longitudinal surface relaxivity parameter
ρ_2 = transverse surface relaxivity parameter
σ_S = surface density of paramagnetic impurities
τ_m = surface correlation time of translation
τ_S = surface residence time
ω = Larmor pulsation
ω_I = proton Larmor pulsation
ω_S = electronic Larmor pulsation
B_0 = external magnetic field
□ = Planck constant divided par 2π
ΔE = effective activation energy
I = nuclear spin
R = gas constant
S = electronic spin
S/V = surface to volume ratio
T = temperature
T_l = laboratory temperature
T_r = reservoir temperature
T_1 = longitudinal relaxation time
T_{1B} = longitudinal relaxation time of the bulk fluid
T_2 = transverse relaxation time
T_{2B} = transverse relaxation time of the bulk fluid
T_{2corr} = transverse relaxation time of the fluid in pores, after the correction of the contribution of bulk fluid
$T_{2cutoff}$ = cutoff transverse relaxation time
$T_{2cutofflab}$ = cutoff transverse relaxation time at the laboratory conditions

Acknowledgment

The authors gratefully thank Dr. R. G. Bryant (university of Virginia, Charlotteville) for his participation in the project and Drs. D. Petit and P. Levitz (École Polytechnique, France) and Dr. G. Chauveteau (IFP, France) for stimulating discussions.

References

1. R. L. Kleinberg, ‘ Nuclear Magnetic resonance’ P.-z. Wong, ed. ‘Experimental methods in the Physics Sciences : Methods of the physics of the porous media’, 1999.
2. Kleinberg, R.L., Well logging, in Encyclopedia of nuclear magnetic resonance: John Wiley and Sons, v. 6, p. 4960-4969, 1996.
3. L. L. Latour, R. L. Kleinberg and A. Sezginer, Nuclear magnetic resonance properties of rocks at elevated temperatures, J. Colloid. Inter. Sc., 150, no 2, pp535-548, 1992.
4. S. Godefroy, J.-P. Korb, M. Fleury, R. G. Bryant, Surface nuclear magnetic relaxation and dynamics of water and oil in macroporous media, To be published in Phys. Rev. E, Aug. 2001.
5. A. Abragam, Principles of Nuclear Magnetism, Clarendon press, Oxford, 1961.
6. I. Foley, S. A. Farooqui,, and R. L. Kleinberg, NMR relaxation of fluids at solid surfaces--effects of paramagnetic ions: J. Magn. Reson., Ser. A, v. 123, (95), 1996.
7. L. E. Cuiec, 'Evaluation of reservoir wettability and its effects on oil recovery', Norman R. Morrow ed., Surfactant science serie, vol. 36, 'Interfacial phenomena in petroleum recovery'.
8. J. Korringa, D. O. Seevers, H. C. Torrey, Theory of spin pumping and relaxation in systems with low concentration of electron spin relaxation centers, Phys. Rev. 127, (4), 1962.
9. R. L. Kleinberg, W. E. Kenyon, and P. P. Mitra, Mechanism of NMR relaxation of fluids in rock: J. Magn. Reson., Ser. A, v. 108, (206),1994.
10. J.-P. Korb, M. Whaley-Hodges, R. G. Bryant, Translational diffusion of liquids at surfaces of microporous materials: theoretical analysis of field-cycling magnetic relaxation measurement, Phys. Rev. E, 56 (2), 1997.
11. J.-P. Korb, M. Whaley Hodges, Th Gobron, and R. G. Bryant, Anomalous surface diffusion of water compared to aprotic liquids in nanopores, Phys. Rev. E, 60, (3), 1999.

12. A. G. Redfield, W. Fite, H. E. Bleich, Precision high speed current regulators for occasionally switched inductive loads. Rev. Sci. Instrum. 39, 710, 1968.
13. V. Médout-Marère, A. El Ghzaoui, C. Charnay, J. M. Douillard, G. Chauveteau and S. Partyka, Surface heterogeneity of passively oxidized silicon carbide particles: Hydrophobic-Hydrophilic partition, J. Colloid interface. Sc., 223, (205), 2000

Appendix. NMR cell for measurements at elevated temperature

A special cell was build for the bench top NMR apparatus used for the measurements at a fixed frequency of 2.2 MHz (MARAN 2 ULTRA equipped with a 51 mm water cooled 1D gradient probe from Resonance Instruments). It allows to perform experiments at a constant temperature varying from 10 up to 100°C. A small and constant pressure (7 Bar) is maintained inside the cell to prevent degassing or boiling of the saturating liquids. The cell is made of two thin concentric tubes build in Peek (Fig. 13) in which a non-hydrogen liquid (Fluorinert^{TM} FC43) is circulating. The temperature of this liquid is maintained at a constant temperature using an external bath. At elevated temperature, the heat losses of the cell are evacuated by (i) the water regulation around the antenna (room temperature of about 22°C) (ii) the air regulation of the magnet (30°C).

The experiments were performed on samples with an optimum diameter and length of 40 and 60 mm respectively. The volume of liquid present between the sample and the cell inner tube is minimized by using a Teflon tape wrapped around the sample. Therefore, there is little perturbation of the sample signal coming from the bulk relaxation of this liquid. Another characteristic of interest is the NMR signal measured on the empty cell. If interpreted as a volume, this signal represents a total of 0.55 cc. The relaxation time of the cell material lies at around 0.2 ms and can be detected only with very short echo spacing and a large number of scans. It has no influence in the present experiments.

The temperature of the sample is known from a calibration curve established with a water filled cell and for various bath temperature. From these tests, the stabilization time (about 1 hour) was also determined, as well as the accuracy of the temperature regulation (estimated to ±1°C). The design of the cell allows performing the long temperature stabilization periods outside the NMR apparatus. When ready, the cell can be placed in the NMR apparatus to proceed with the relaxation measurements.

Table 1. Variation of T_2 of water saturating the Clashash sandstone

Temperature °C	T_2 peak (ms)	T_{2corr} (ms)
26	800	1137
52	670	779
70	600	656
89	565	600

Table 2. Variation of T_2 of water saturating the reservoir sandstone

Temperature °C	T_2 peak (ms)	T_{2corr} (ms)
26	710	963
52	660	765
70	620	680
86	595	633

Table 3. Variation of T_2 of water saturating the reservoir carbonate

Temperature °C	T_2 peak (ms)
26	87
38	92
52	101
75	122
89	142
96	153

Table 4. Resume of the measured effective activation energies, of water and oil (dodecane) in bulk, or saturating the different porous media

Material	Water DE kcal/mol	Oil DE kcal/mol
Bulk liquid	4.5	2.6
SiC grain packing	-2	2
Calcite grain packing	1.9	
Clashash sandstone	-2	
Reservoir sandstone	-1.7	1.5
Lavoux limestone	2.5	
Reservoir carbonate	1.9	2.4

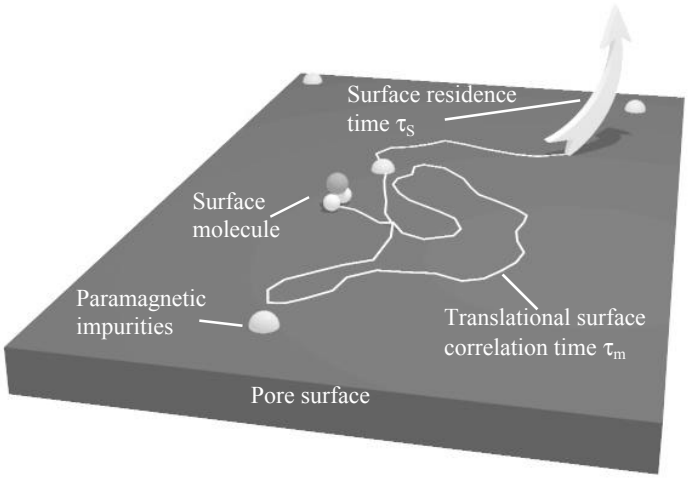

Fig. 1-Model of the two-dimensional translational diffusion of the proton species at the pore surface. The spin-bearing molecules (for example, water) diffuse at the surface, sometimes reaching fixed surface paramagnetic impurities where the spins relax. The translational surface correlation time is defined as t_m. This surface motion is interrupted by the surface desorption, characterized by a surface residence time t_S.

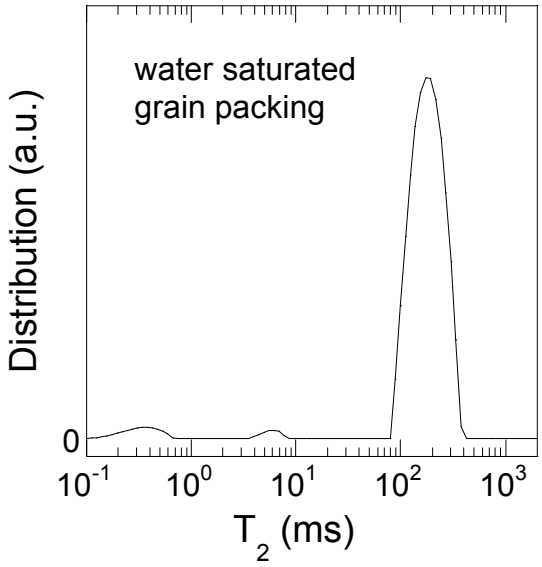

Fig. 2-Distribution of relaxation times T_2 of a packing of silicon carbide grains of 8 μm of diameter, saturated with water.

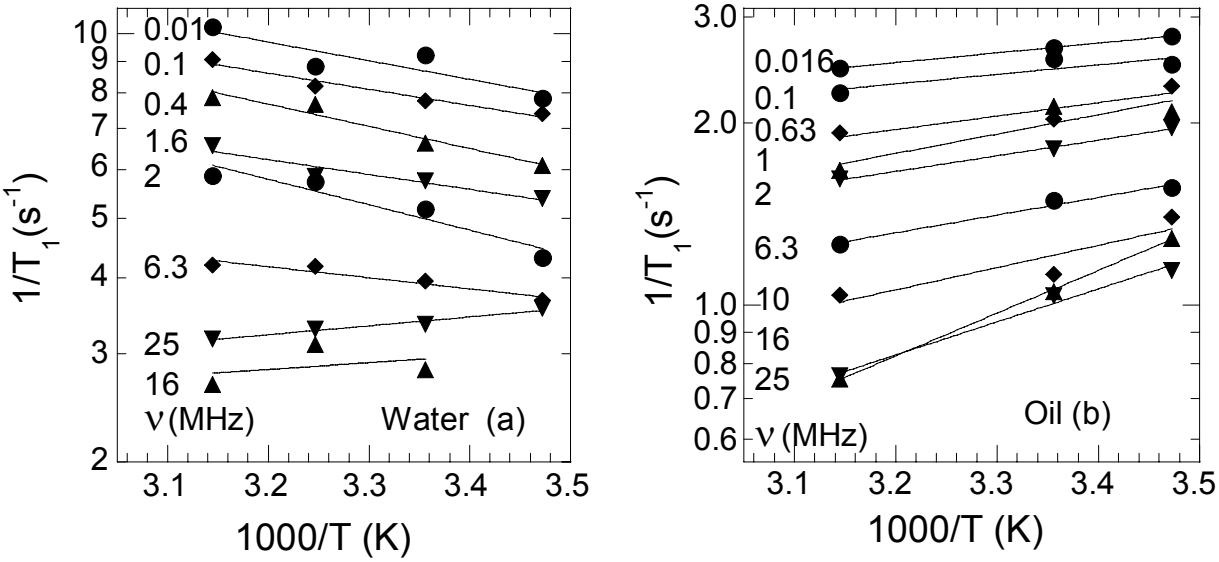

Fig. 3-Arrhenius diagrams of the measured relaxation rates of liquids saturating the 8 µm grain packing, as a function of the inverse of temperature, 1000/T, for different proton Larmor frequencies, ν (a) for water and (b) for oil.

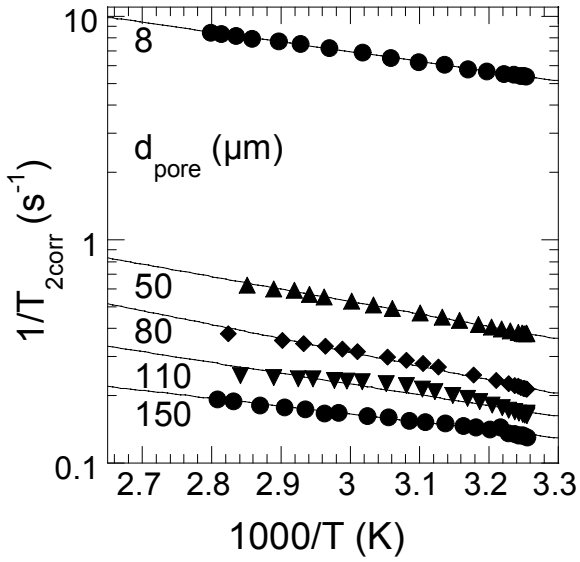

Fig. 4-Arrhenius plot of the variation of the mean transverse relaxation rates, $1/T_2$, as a function of the inverse of the temperature, 1000/T, of water saturating the packing of different grain size, varying in the series {8, 50, 80, 110 and 150 µm}. The measured temperature variation is opposed to the water one's. One measures an activated energy $\Delta E \approx -2$ kcal/mol.

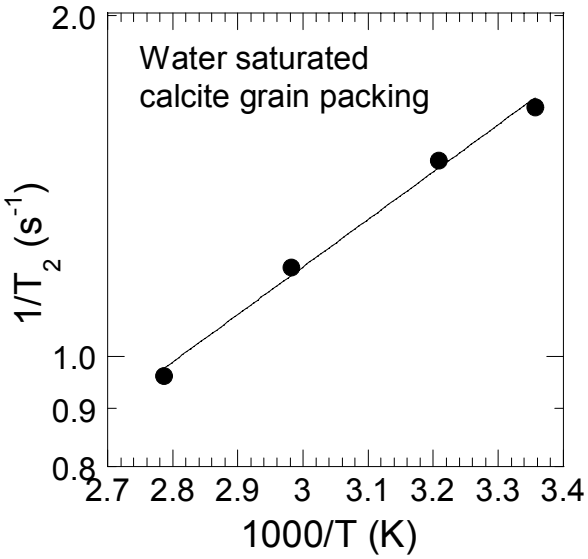

Fig. 5-Arrhenius diagram of the variation of the measured transverse relaxation rate, $1/T_2$, as a function of the inverse of the temperature, 1000/T, of water saturating the calcite grain packing. One measures an effective activation energy of 1.9 kcal/mol.

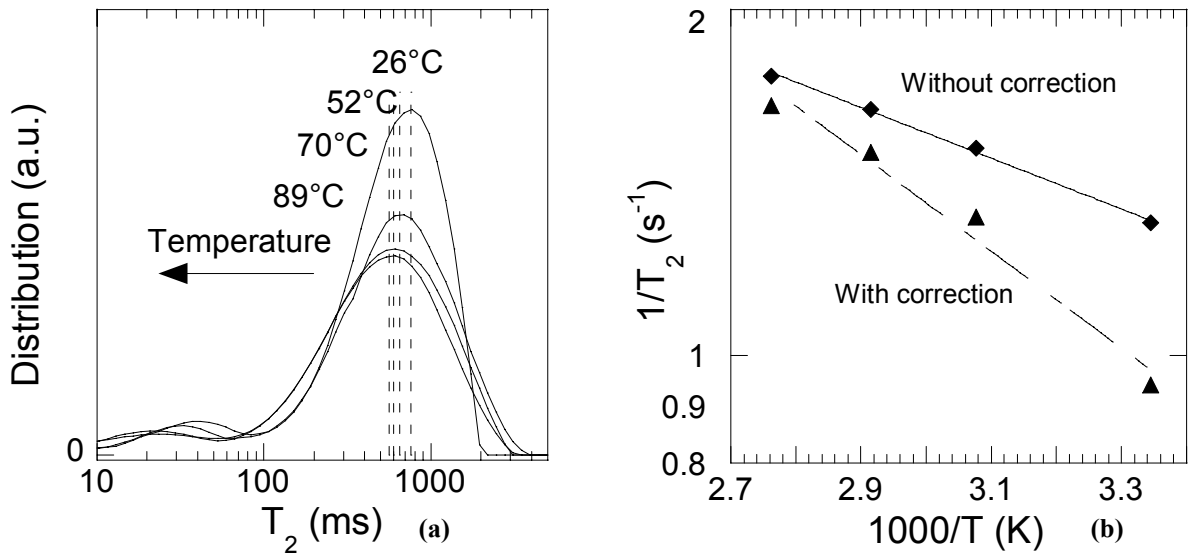

Fig. 6-(a) Variation of the transverse relaxation time distribution, T_2, as a function of the temperature, of water saturating a Clashash sandstone. One notes that T_2 decrease with increasing temperature. (b) Arrhenius plot of the variation of the mean measured, $1/T_2$, (◆) and corrected from the bulk contribution (Eq. (5)), $1/T_{2corr}$, (▲) transverse relaxation rates as a function of the inverse of the temperature, 1000/T, of water saturating a Clashash sandstone. One notes a temperature variation in opposition to the bulk water one's, with a measured effective activation energy of -2 kcal/mol.

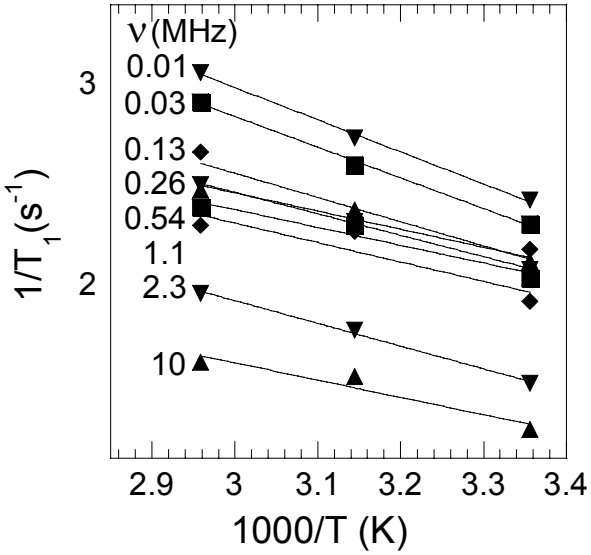

Fig. 7-Arrhenius diagrams of the measured longitudinal relaxation rates, $1/T_1$, of water saturating a Clashash sandstone, as a function of the inverse of temperature, 1000/T, and for different Larmor frequencies ν.

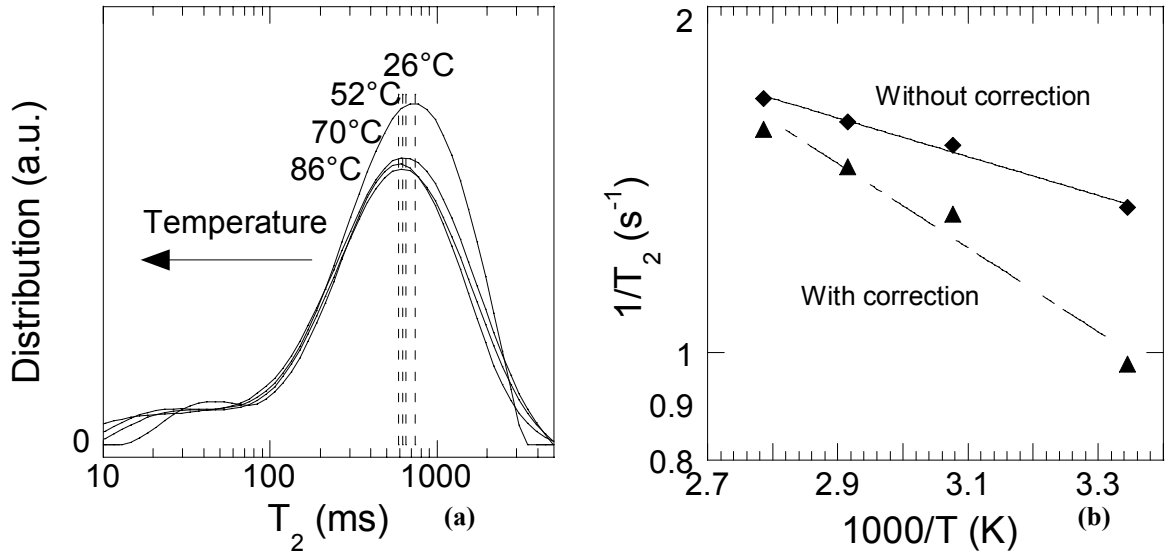

Fig. 8-(a) Variation of the transverse relaxation time distribution, T_2, as a function of the temperature, of water saturating a reservoir sandstone. One notes that T_2 decrease with increasing temperature. (b) Arrhenius plot of the variation of the mean measured, $1/T_2$, (◆) and corrected from the bulk contribution (Eq. (5)), $1/T_{2corr}$, (▲) transverse relaxation rates, as a function of the inverse of the temperature, 1000/T, of water saturating the reservoir sandstone. One notes a temperature variation in opposition to the bulk water one's, with a measured effective activation energy of -1.7 kcal/mol.

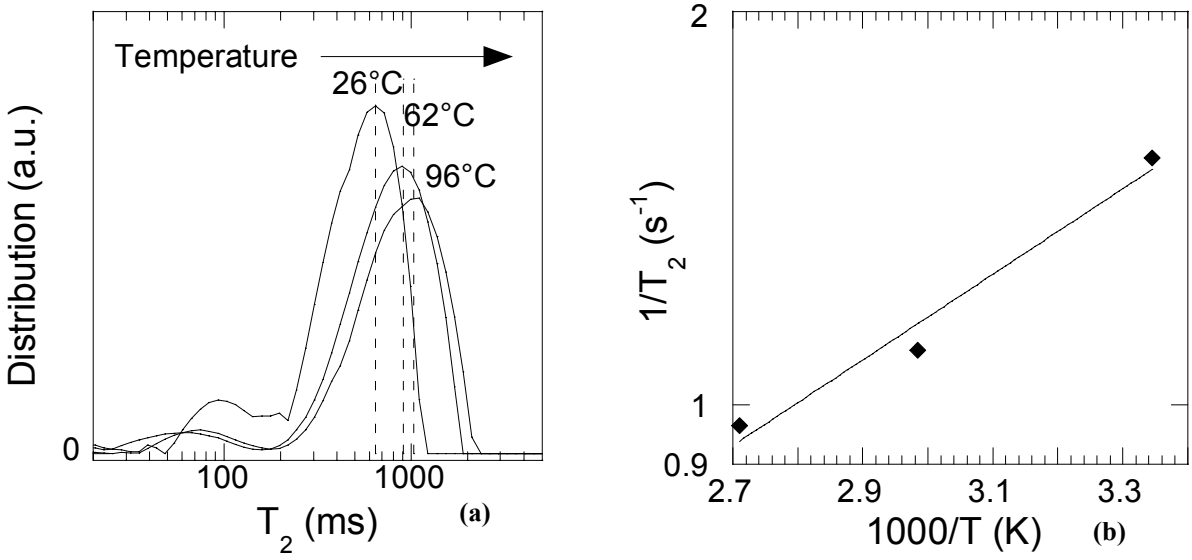

Fig. 9-(a) Variation of the transverse relaxation time distribution, T_2, as a function of the temperature, of oil (dodecane) saturating a reservoir sandstone moderately oil wet (Iw=-0.19). One notes that T_2 increase with increasing temperature. (b) Arrhenius plot of the variation of the mean measured transverse relaxation rates, $1/T_2$, as a function of the inverse of the temperature, 1000/T, of water saturating the reservoir sandstone.

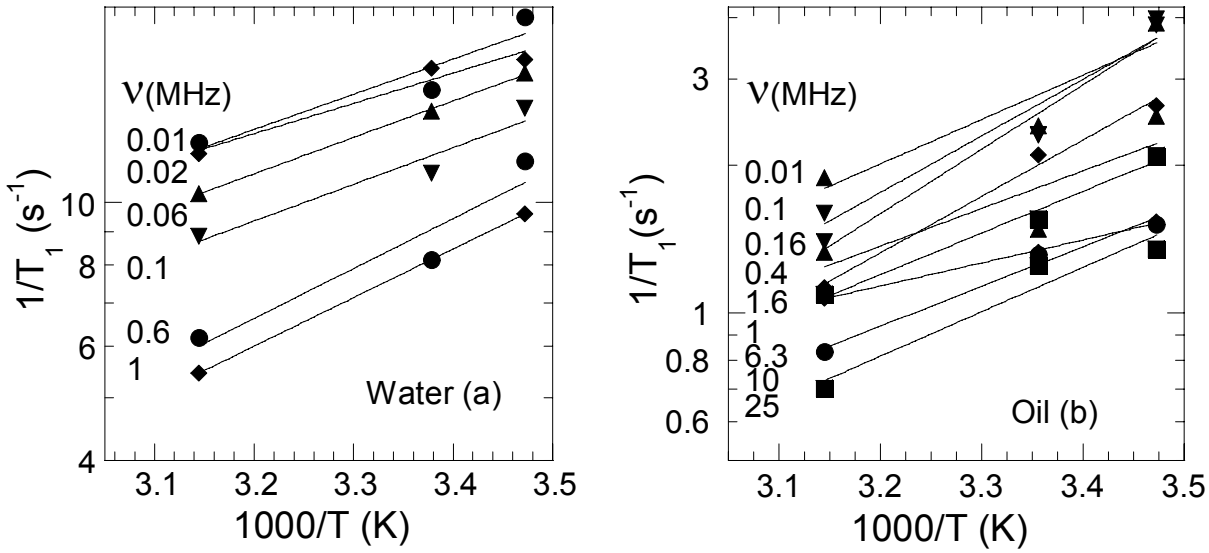

Fig. 10-Arrhenius diagrams of the measured relaxation rates of liquids saturating a limestone rock (Lavoux), as a function of the inverse of temperature, 1000/T, for different proton Larmor frequencies, ν (a) for water and (b) for oil.

-

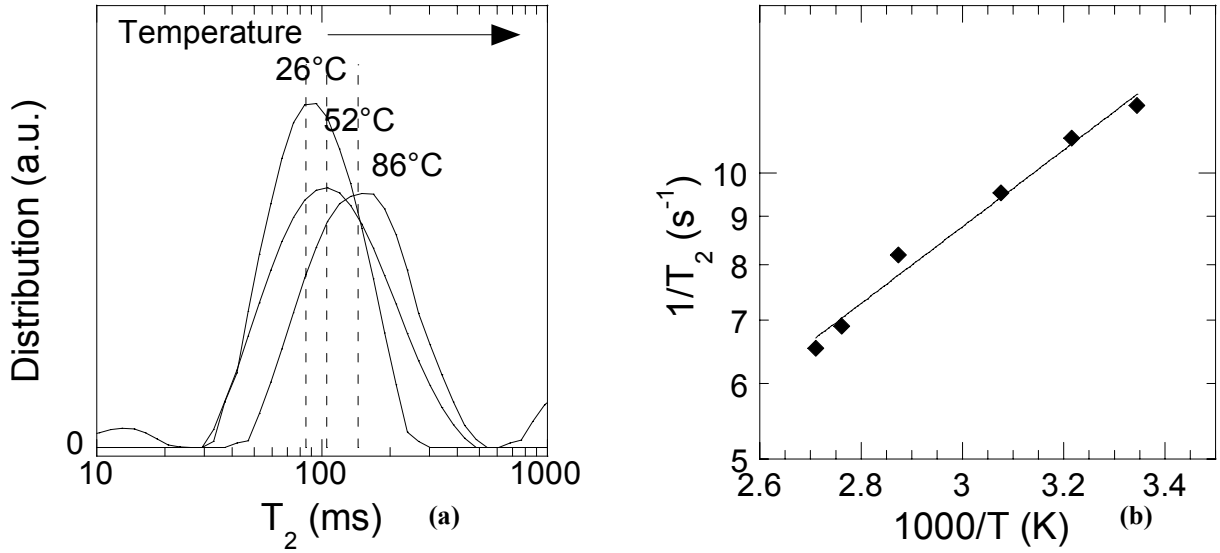

Fig. 11-(a) Variation of the transverse relaxation time distribution, T_2, as a function of the temperature, on water saturating a reservoir carbonate moderately water wet (Iw=+0.50). (b) Arrhenius diagram of the variation of the mean transverse relaxation rates, $1/T_2$, as a function of the inverse of the temperature, 1000/T, on the water saturated reservoir carbonate. One notes an activated process, with a measured activation energy of 1.9 kcal/mol.

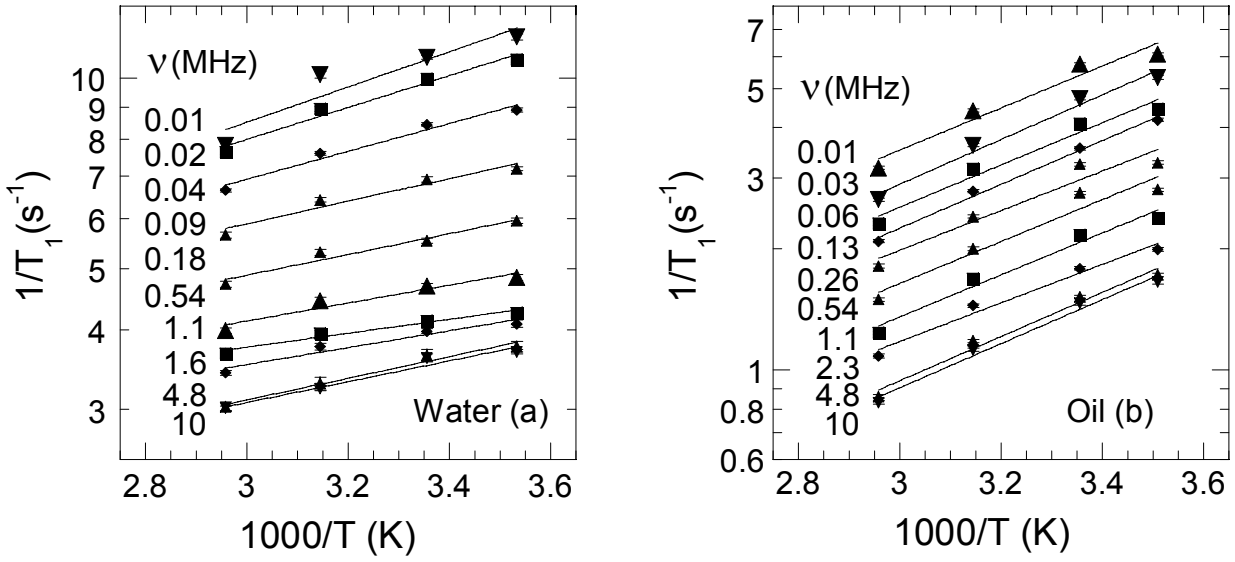

Fig. 12-Arrhenius diagrams of the measured relaxation rates of liquids saturating a reservoir carbonate moderately water wet (Iw=+0.50), as a function of the inverse of temperature, 1000/T, for different proton Larmor frequencies, ν (a) for water and (b) for oil.

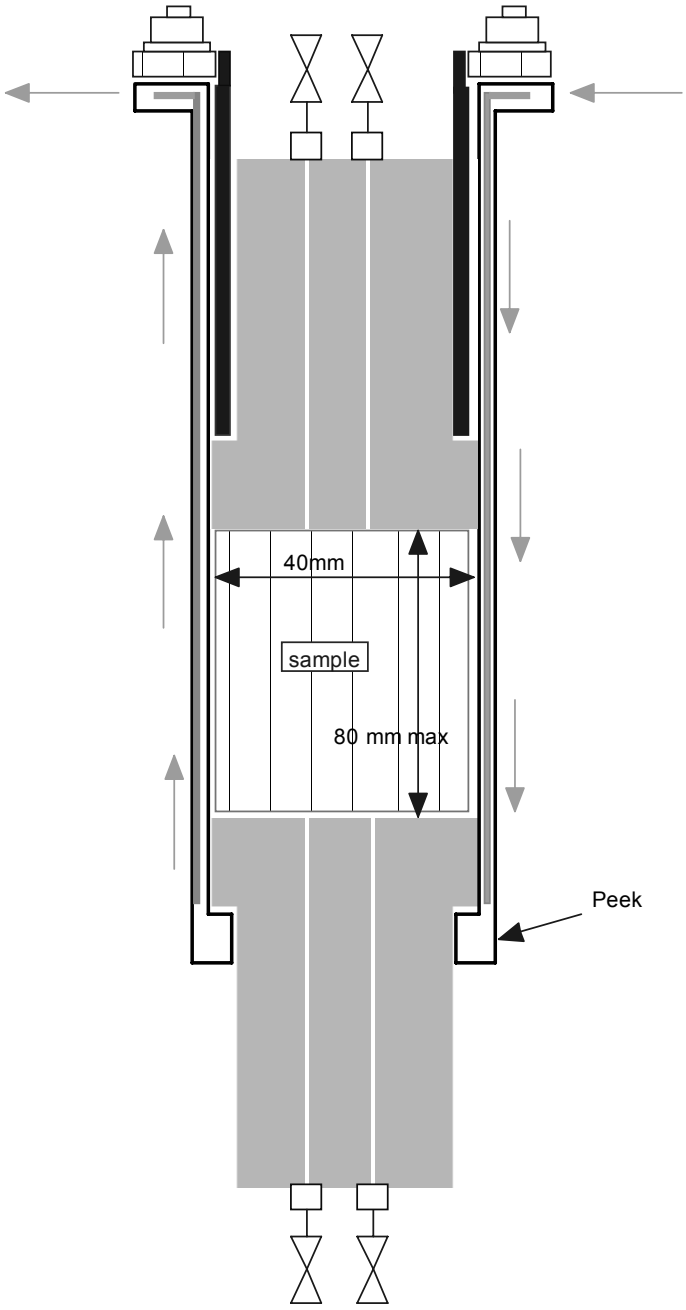

Fig. 13-Temperature regulated NMR cell (IFP design) for measuring NMR properties at various temperatures (from 10 up to 100°C). The outer diameter of the cell is 51 mm. A maximum pressure of 10 Bar can be applied to prevent degassing or boiling of the saturating liquid. The optimum length of the sample is 60 mm.